ISPRS Open Journal of Photogrammetry and Remote Sensing 13 (2024) 100071

Contents lists available at ScienceDirect

ISPRS Open Journal of Photogrammetry and Remote Sensing

journal homepage: www.journals.elsevier.com/isprs-open-journal-of-photogrammetry-and-remote-sensing

Individual tree detection and crown delineation in the Harz National Park from 2009 to 2022 using mask R–CNN and aerial imagery

Moritz Lucas [a,b,*], Maren Pukrop [a,b], Philip Beckschäfer [c], Björn Waske [a,b]

[a] Joint Lab Artificial Intelligence and Data Science, Osnabrück University, Osnabrück, Lower Saxony, Germany
[b] Working Group Remote Sensing and Digital Image Analysis, Osnabrück University, Osnabrück, Lower Saxony, Germany
[c] Northwest German Forest Research Institute, Göttingen, Lower Saxony, Germany

ARTICLE INFO

Keywords:
Remote sensing
Forest monitoring
Deep learning
Object detection
Photogrammetry

ABSTRACT

Forest diebacks pose a major threat to global ecosystems. Identifying and mapping both living and dead trees is crucial for understanding the causes and implementing effective management strategies. This study explores the efficacy of Mask R–CNN for automated forest dieback monitoring. The method detects individual trees, delineates their crowns, and classifies them as alive or dead. We evaluated the approach using aerial imagery and canopy height models in the Harz Mountains, Germany, a region severely affected by forest dieback. To assess the model's ability to track changes over time, we applied it to images from three separate flight campaigns (2009, 2016, and 2022). This evaluation considered variations in acquisition dates, cameras, post-processing techniques, and image tilting. Forest changes were analyzed based on the detected trees' number, spatial distribution, and height. A comprehensive accuracy assessment demonstrated the Mask R–CNN's robust performance, with precision scores ranging from 0.80 to 0.88 and F1-scores from 0.88 to 0.91. These results confirm the model's ability to generalize across diverse image acquisition conditions. While minor changes were observed between 2009 and 2016, the period between 2016 and 2022 witnessed substantial dieback, with a 64.57% loss of living trees. Notably, taller trees appeared to be particularly affected. This study highlights Mask R–CNN's potential as a valuable tool for automated forest dieback monitoring. It enables efficient detection, delineation, and classification of both living and dead trees, providing crucial data for informed forest management practices.

1. Introduction

The Harz Mountains, as the northernmost mountain range in Germany, contain the Harz National Park, where historical forestry practices have resulted in the predominance of one or very few tree species (Knapp et al., 2013). In recent years, this ecosystem has been threatened due to the forest structure, a severe drought, and subsequent bark beetle attacks, resulting in widespread forest dieback (Thonfeld et al., 2022; Holzwarth et al., 2023). To gain a sophisticated understanding of these developments and support decision-making, the implementation of an earth-observation based forest monitoring system becomes crucial (Holzwarth et al., 2020, 2023). Currently, the primary tools for forest monitoring in the national park include in situ measurements and manual interpretation of aerial imagery (Harz National Park, 2023a). Besides, analyzing satellite, aerial, or drone imagery as well as laser scanning enables cost-effective and regular forest monitoring (Bagheri and Kafashan, 2023; Zhen et al., 2016; Nduji et al., 2023). Individual Tree Detection and Crown Delineation (ITDCD) is a popular approach for forest monitoring, as it provides a precise representation of the forest, enabling tree counting and provision of, for example, tree height or above-ground biomass (Chadwick et al., 2020; Sun et al., 2022, 2023; Jaskierniak et al., 2021). Several traditional algorithms, such as valley-following, region-growing and watershed segmentation, are used for ITDCD (Zhao et al., 2023a; Mohan et al., 2017; Minařík et al., 2020).

Recently, Convolutional Neural Networks (CNN) have been increasingly used to perform ITDCD (Zhao et al., 2023b). Mask Region-based Convolutional Neural Networks (Mask R–CNN) are particularly interesting in this context, as they are able to detect, delineate and classify objects. Furthermore, trees are recognized not only by spectral reflectance and geometrical information but also by spatial patterns and neighborhood relationships (He et al., 2020). In comparison to traditional methods, Mask R–CNN has shown better results performing ITDCD (Yu et al., 2022; Zhao et al., 2023b). It has been widely used to detect individual trees in plantations (Safonova et al.,

* Corresponding author. Joint Lab Artificial Intelligence and Data Science, Osnabrück University, Osnabrück, Lower Saxony, Germany.
E-mail address: moritz.lucas@uos.de (M. Lucas).

https://doi.org/10.1016/j.ophoto.2024.100071
Received 29 January 2024; Received in revised form 6 June 2024; Accepted 19 June 2024
Available online 5 July 2024

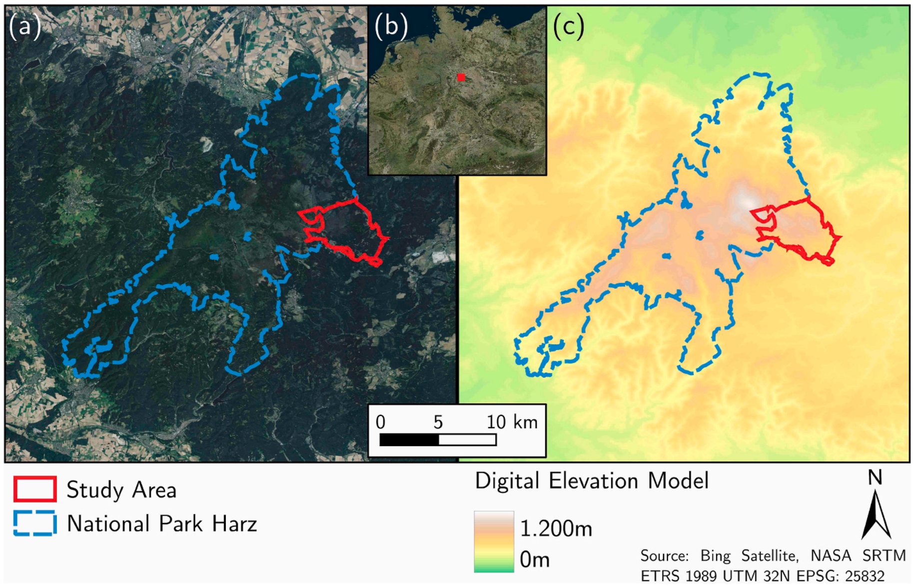

Fig. 1. The study area and the Harz National Park and its surroundings on (a) imagery from Bing Satellite (c) the SRTM DTM from NASA. (b) The map frame of (a) and (c) in Germany.

2021), urban forests (Sun et al., 2022), natural deciduous (Braga et al., 2020) and coniferous forests (Chadwick et al., 2020). The results in Gibril et al. (2022) and Dersch et al. (2023) showed that Mask R–CNN outperformed other CNN- or Transformer-based instance segmentation models. However, trees in very dense forests characterized by a variety of tree species and overlapping crowns are much more difficult to detect and delineate than trees in plantations (Zhao et al., 2023a). While most of these studies focus on a relatively small area with the use of drone images (Zhao et al., 2023b), as this offers the highest spatial resolution, other studies used very high-resolution satellite imagery (Wagner et al., 2018; Lassalle et al., 2022) or aerial imagery (Yang et al., 2022). Although the mapping accuracy can be reduced due the lower spatial resolution of the data (Zhao et al., 2023a), these data can provide temporally frequent information on the environmental state over wide and remote areas (Ke and Quackenbush, 2011). As input for the Mask R–CNN in the ITDCD task Red, Green, Blue (RGB) channeled images are the most common, as these are the cheapest to capture and the CNN structure is designed to process three channeled images (Zhao et al., 2023a). Nevertheless, adding digital aerial photogrammetry (Lucena et al., 2022) or LiDAR-generated Canopy Height Models (CHM) (Li et al., 2022) and Near-Infrared (NIR) channels can increase accuracy (Hao et al., 2021). In most cases, ITDCD classifies all living trees in a single class (Sun et al., 2022). For more specific applications, dead trees (Chiang et al., 2020) or specific tree species (Mielczarek et al., 2023) can be detected within the forest. Other studies have used multiple classes and distinguished between tree species (Zhang et al., 2022; Sandric et al., 2022) or health conditions (Safonova et al., 2019; Nguyen et al., 2021; Minařík et al., 2020).

The proposed study is focusing on detecting alive and dead trees to specifically assess the development during a forest dieback. As forest development in the Harz National Park has not yet been analyzed by remote sensing studies and a forest dieback has currently occurred, it shows a valuable case study. Many forestry administrations have been carrying out aerial surveys for decades, these are widely available and could therefore used for long-term forest monitoring. These surveys are carried out by different contractors, so the acquisition dates, cameras, post-processing and tilting effects differ. Therefore, aerial imagery from the years 2009, 2016 and 2022 was provided by the Harz National Park to investigate forest changes. The following research questions arise from these conclusions:

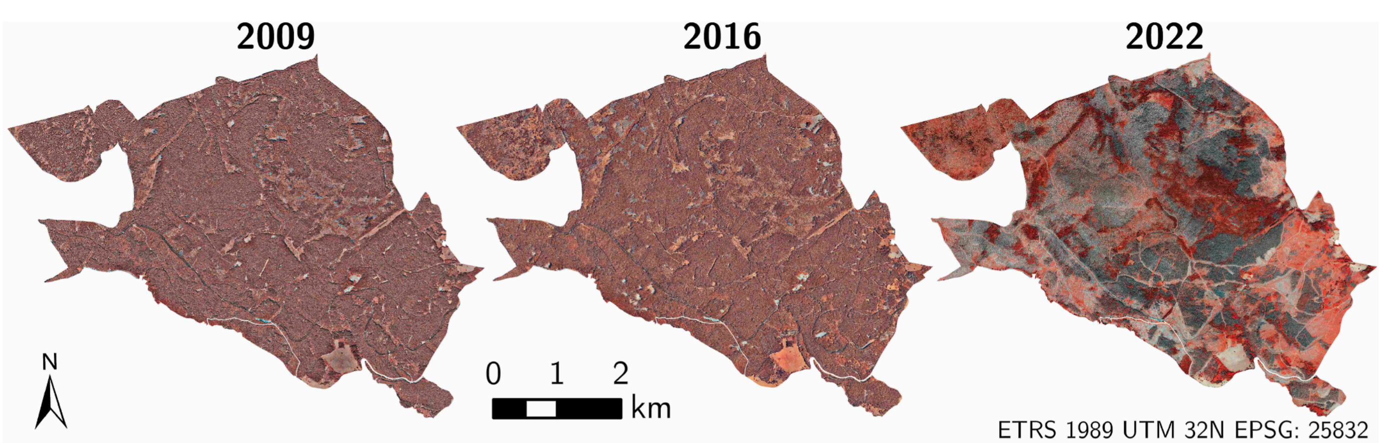

Fig. 2. False colour composites of the 2009, 2016 and 2022 aerial imagery within the boundaries of the study area. (For interpretation of the references to colour in this figure legend, the reader is referred to the Web version of this article.)

Table 1
Metadata of the aerial imagery from 2009, 2016 and 2022. Date and time of recording, the camera used, overlap long and cross flight direction, ground sampling distance (GSD) and zenith angle of the sun during flight.

	Date of recording	Camera	Overlap long/cross	GSD	Sun angle
2009	20.08.2009 11:38–14:26	Intergraph DMC 01 Nr.113	70%/40%	20 cm	45°–51°
2016	23.06.2016 09:40–11:15	DMCII_250	60%/30%	20 cm	40°–60°
2022	24.08.2022 08:34–11:15	UltraCam Eagle M3	80%/30%	20 cm	38°–49°

Table 2
Number of manual delineated tree crowns for training and validation.

	Training			Validation		
	Alive	**Dead**	**Total**	**Alive**	**Dead**	**Total**
2009	1720	157	1877	173	186	359
2016	3557	1222	4779	473	106	579
2022	1327	1220	2547	173	186	359
Total	**6604**	**2599**	**9203**	**1235**	**350**	**1585**

- What accuracy can be achieved for individual tree detection and crown delineation and classification as alive or dead using Mask R–CNN?
- Is a Mask R–CNN suitable for detecting individual trees in aerial imagery with differing cameras, dates, post-processing and tilting effects?
- Which forest changes can be detected in the Harz Mountains between 2009 and 2022 using aerial imagery?

The paper is structured as follows: first, the study area in the Harz Mountains, the datasets consisting of aerial images and reference data for training and validating the model are described. Afterwards, methods underlying the individual tree detection and crown delineation are presented. Then the results including the accuracy assessment of the tree detection and the forest changes are described. Finally, the results placed within the current research context, the limitations of the methodology are described and reasons for the forest development are discussed.

2. Study area and datasets

2.1. Study area: The Harz Mountains

The study area is located within the Harz Mountains and is part of the Harz National Park, which was established in 2006 (Harz National Park, 2023b). The study area covers an area of 2181ha, stretching from north to south for about 6km and from west to east for about 8km (Fig. 1). The area is situated on the eastern slopes of the Brocken, the highest peak in the mountain range at 1141m. It is located at an altitude of 500–1000m, which, under natural circumstances, would be dominated by beech with a transition to spruce at an altitude of 700–800m. Towards 1100m, the spruce forest opens up to the timberline (Schmidt et al., 2022; Kison et al., 2020). However, due to previous forestry use, spruces were planted because of their ability to grow fast in the adverse climate, making this species dominant. This dominance has declined in recent years in favor of beech (Harz National Park, 2022). In addition, the area is crisscrossed by bogs, scree slopes and forest trails. The climate in the study area is particularly wet, with an average annual precipitation of 1245mm and cold, with an average annual temperature of 5.9°C, compared to the surrounding lowlands (Deutscher Wetterdienst, 2023a, b). In the study period (2009–2022), the climate has been substantially warmer (6.9°C) and drier (1133mm) than the long-term average

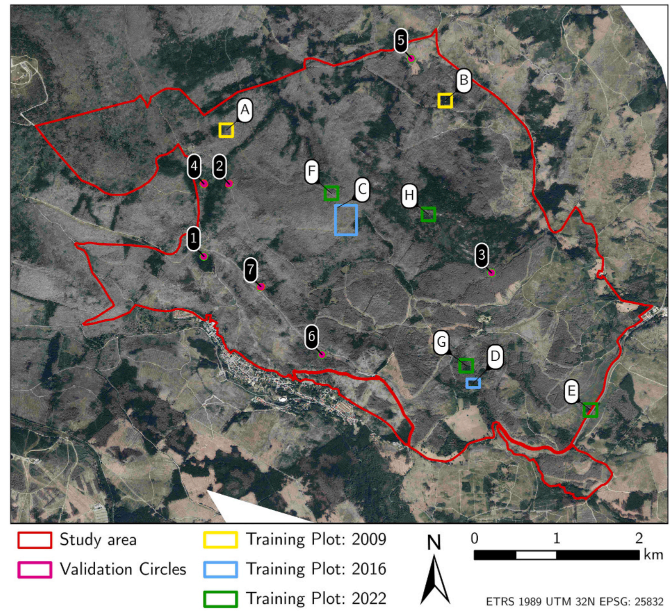

Fig. 3. Distribution of training (blue, green and yellow) and validation (pink) plots on aerial imagery from 2022 within the study area. Details of the plots can be seen for training in Fig. A.10 and for validation in Fig. A.11. (For interpretation of the references to colour in this figure legend, the reader is referred to the Web version of this article.)

(Deutscher Wetterdienst, 2023a,b) (see Fig. 2).

2.2. Aerial imagery

The aerial imagery used in this study is based on three surveys conducted in the years 2009, 2016 and 2022 (Table 1 and Fig. 2). All images were captured during the summer months between June and August, with a spatial resolution of 20 cm and included RGB and NIR bands. However, overlap ratios and cameras varied during the flight campaigns. Additionally, varying acquisition times and sun zenith angles resulted in different illumination conditions.

To create orthophotos, aerotriangulation and digital orthomosaic creation in 2009 and 2016 were carried out with *IMAGINE Photogrammetry* from *Hexagon AB* (Stockholm, Sweden), while *MATCH-AT* from *Trimble Inc.* (Sunnyvale CA, USA) was used in 2022. To ensure data comparability, all orthomosaics were resampled to a resolution of 0.2m using nearest neighbor and all band values were scaled from 0 to 255. To create the CHM, a digital surface model (DSM) was calculated from raw aerial images with their orientation parameters and a digital terrain model (DTM) using *Match-T DSM* from *Trimble Inc.* (Sunnyvale CA, USA). Which uses cost-based matching, which combines semi-global matching algorithms with feature-based matching algorithms and is recommended for non-man-made objects (Trimble, 2019). The resulting point clouds yielded good internal height accuracies: 2009: 0.2m, 2016: 0.24m, and 2022: 0.16m. Filtering and rasterizing these point clouds was derived from the ”Flächendeckende Fernerkundungsbasierte Forstliche Strukturdaten (F^3)” project, which is optimized for deriving CHM from aerial imagery for forestry applications (Kirchhöfer et al., 2020b).

2.3. Reference data

Two independent tree crown datasets were required to train and test the Mask R–CNN and to validate the results. To prepare the training dataset, different plots were defined for each year in the investigation period. These plots were chosen to ensure as much variability as possible in the data. This variability encompassed coniferous and deciduous trees, as well as standing deadwood at varying tree heights and

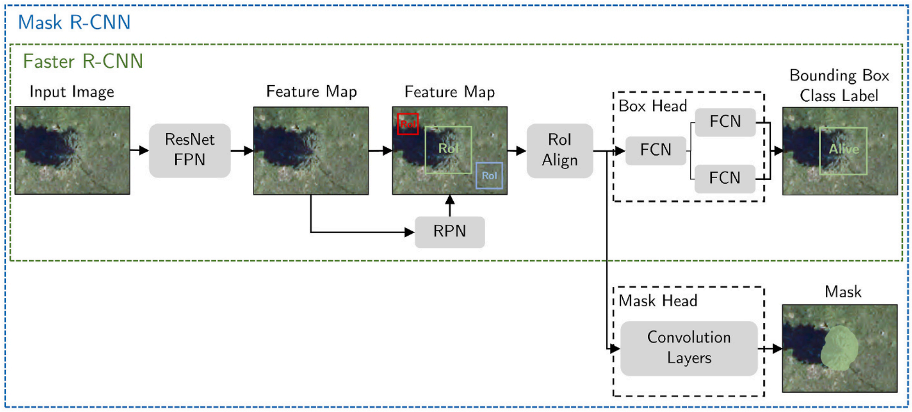

Fig. 4. The Mask R–CNN architecture.

background elements such as paths, bare ground, fallen trees and understory. The resulting plots are visualized in Fig. 3, with detailed representations provided in the Fig. A.10. For the validation dataset seven circular validation polygons with a 50m diameter were placed to include both alive and dead trees across each year. The manual delineation and labeling of each individual tree crown within the training polygons for the corresponding year, and across all years for the validation polygons, were executed through visual interpretation of orthophotos. Here the assumption was made that each tree is either dead or alive; in borderline cases, the tree was assigned to the closest category.

The ensuing validation plots can be seen in Fig. 3 and a detail of the RGB composite from each year in Fig. A.11. The total number of delineated tree crowns in the training and validation datasets is shown in Table 2.

3. Methods

3.1. Mask R–CNN

Mask R–CNN is a deep learning model that is commonly used for object detection tasks in remote sensing (Li et al., 2020), particularly for ITDCD tasks (Braga et al., 2020; Hao et al., 2021; Zhang et al., 2022; Safonova et al., 2021). The structure of the Mask R–CNN (Fig. 4) builds upon the Faster R–CNN by adding a branch that predicts a binary mask for each detected object (He et al., 2020; Ren et al., 2017). As a first step, equal-sized input images are inserted into the Residual neural Network (ResNet) and Feature Pyramid Network (FPN) backbone structures, which perform multiple convolutional and pooling tasks to extract visual feature maps at different scales. These features are used as input to the Region Proposal Network (RPN), which creates proposed Regions of Interests (RoI). RoIAlign operation extract these proposed RoIs in a fixed-size using bilinear interpolation. In the box head, Fully Connected Networks (FCN) perform the RoI classification to determine the class label and a refined bounding box. In the mask head pixel-level masking is carried out by convolutional layers in the respective RoI (He et al., 2020). The network is trained using backpropagation and mini-batch stochastic gradient descent (He et al., 2020). The Mask R–CNN model was performed with the ArcGIS (Version 3.0.0) API for Python, using an implementation from He et al. (2020) with Fast.ai and PyTorch.

3.2. Training data and model training

To train the Mask R–CNN, fixed-sized image chips of the aerial imagery merged with the CHM and binary masks for each class were required. The size of the image chips was set to 256 × 256 pixels (2,621m^2) with a overlap of 75%, thereby RGB, NIR, and CHM bands were used. Attaching the CHM and NIR bands has already been proven to increase performance for ITDCD (Lucena et al., 2022; Hao et al., 2021; Li et al., 2022; Schiefer et al., 2020). The image chips were created only within the training plots described in section 2.3, to ensure that the training data included only labeled trees. The tree crown polygons were used to create R–CNN masks for the classes alive and dead tree crowns. Due to the high overlap, a total of 956 image chips were created over the investigation period (Table 3). From this sample, 765 (80%) were used for the Mask R–CNN training and 191 (20%) were used for testing during training.

ResNet-50 was used as pretrained backbone to train the Mask R–CNN, as this has been shown to lead to more robust results in ITDCD (Hao et al., 2022). A learning rate finder was used to determine the learning rate (Smith, 2017), which finds the learning rate value that generated the lowest loss after a series of small runs. The training was started with a learning rate of 1.5849e^{-04} and a batch size of 4. While training, augmentation was randomly applied to the training and validation images before feeding them into the neural network. Three types of data augmentation were implemented: vertical flip with a probability of 50%, rotation from 180° to −180° with a probability of 50% and brightness change from a range from 40% to 140%.

The training lasted for 500 epochs, but the validation loss reached its lowest value after 463 epochs (1.42) (Fig. 5). Therefore, the model saved in this state was used for the following ITDCD.

Table 3
Number of image chips per year and class used for Mask R–CNN training. Note that one image chip can have multiple labels.

Year	Alive	Dead	Total
2009	160	80	162
2016	470	402	470
2022	264	313	324
Total	**894**	**795**	**956**

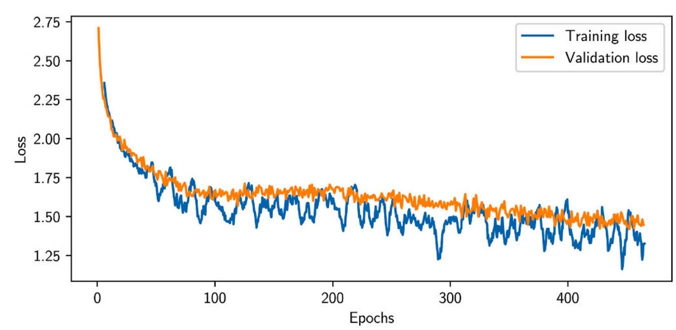

Fig. 5. Development of training and validation losses during training of the Mask R–CNN.

Table 4
Description of the forest parameters and their calculation methods applied for validation.

Forest Parameter	Description
Total	Total number of tree crowns with centroids in the plot
% Dead	Percentage of dead trees of the total number above
Height	Mean of maximum height of CHM within tree crown
% Gap	Percentage of the plot that is not covered by tree crowns

3.3. Tree crown detection and delineation

The trained model was applied to the aerial imagery from 2009, 2016 and 2022, in order to detect individual tree crowns and classify them as either alive or dead. The model's output consists of vector files, each containing with corresponding class annotations and confidence scores. Any tree crowns with a confidence score below 0.2 are discarded (Hao et al., 2022). The non-maximum suppression algorithm was applied to remove features overlapping more then 30% to another (Wu and Li, 2021). In order to quantify forest changes, the number and height of dead as well as alive trees is shown for 2009, 2016 and 2022. For the tree heights the maximum CHM values in each tree crown is utilized.

3.4. Accuracy assessment

For an independent validation of the results, a detailed accuracy assessment was performed. Intersection over Union (IoU), a widely used metric, was employed for the comparative analysis of tree crown detection results against the reference data obtained from the validation plots. IoU is calculated by dividing the intersecting area of the detected tree crown and the reference tree crown by the union area (Padilla et al., 2020). An IoU threshold of 0.5 is used to distinguish a detected tree crown as true positive (TP), as this is a commonly used threshold (Maxwell et al., 2021). Based on the IoU, additional accuracy metrics were derived, including Precision, Recall and the F1-Score. Additionally, the Average Precision (AP) is calculated for an IoU of 0.5. AP is a single scalar value that summarizes the precision-recall curve and provides a measure of the overall performance of the object detection model. To test the reliability of the detection the F1-Score is tested at IoU thresholds ranging from 0.5 to 0.95.

$$AP = \int_0^1 Precision(Recall)\ dRecall \tag{1}$$

These accuracy metrics were calculated for all years and both classes, and for the classes combined. To account for the algorithm's performance in different environments, the performance and forest parameters were calculated for each individual validation polygon in each year. This analysis enables investigating the impact of different forest compositions and backgrounds on accuracy. Forest composition was described using several forest parameters derived within the validation plots, based on the ground truth tree crowns. These parameters and their calculation methods are described in Table 4. Finally, the dominant background types were interpreted and annotated from respective aerial imagery.

4. Results

4.1. Accuracy of tree crown detection and delineation

Fig. 6 shows a close-up of the same area, displaying the detected alive and dead tree crowns in 2009, 2016 and 2022. Table 5 summarizes F1-Score and AP for all three years. We can see that both metrics achieved their highest values in 2016 (0.93 F1-Score, 0.88 AP), followed by 2009

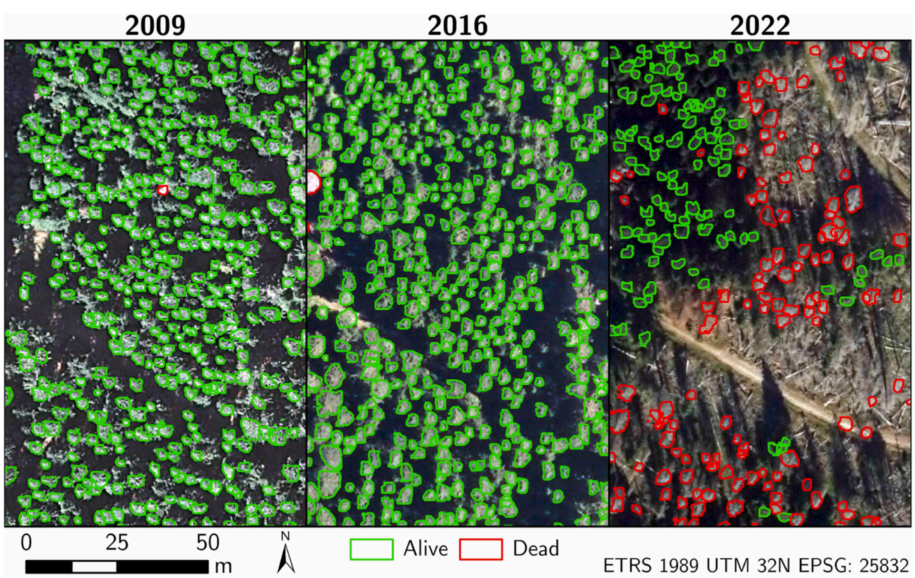

Fig. 6. Detail of the same area, displaying the detected alive and dead tree crowns in 2009, 2016 and 2022 with the respective aerial imagery.

Table 5
Accuracy metrics: Recall, Precision, F1-Score and Average Precision (AP) for each year, for each class and for both classes combined with an Intersection over Union value of 0.5.

	2009			2016			2022		
	Alive	**Dead**	**Total**	**Alive**	**Dead**	**Total**	**Alive**	**Dead**	**Total**
Precision	0.95	0.85	0.94	0.97	0.93	0.96	0.91	0.85	0.88
Recall	0.89	0.96	0.89	0.89	0.93	0.90	0.87	0.90	0.88
F1-Score	0.92	0.90	0.91	0.93	0.93	0.93	0.89	0.87	0.88
AP	0.81	0.70	0.80	0.88	0.90	0.88	0.83	0.80	0.81

Table 6
Description validation plots in 2009, 2016 and 2022 using **F1-Score**, **Precision**, **Recall**, **Total**: Number of ground truth trees and in brackets of detected trees, **% Dead**: Fraction of ground truth dead trees, **Height**: Mean value of all maximum CHM values of the ground truth tree crowns, **% Gap**: Gap percentage and **Background**: Background composition: 1: Shadow, 2: Lying deadwood, 3: Bare ground, 4: Shrubs and grass (Ascending from most to least frequent).

	1	2	3	4	5	6	7
	2009						
F1-Score	0.95	0.88	0.84	0.92	0.94	0.92	0.93
Precision	0.97	0.89	0.91	0.89	0.99	0.97	0.90
Recall	0.94	0.86	0.78	0.96	0.90	0.87	0.96
Total	121 (118)	73 (71)	93 (80)	70 (75)	98 (89)	119 (106)	73 (78)
% Dead	0	5	0	0	0	0	74
Height	9.82	21.28	8.31	26.45	19.88	22.36	31.38
% Gap	66	69	72	60	65	63	65
Background	1, 4	1	4	1	1	1	1
	2016						
F1-Score	0.93	0.91	0.96	0.89	0.94	0.95	0.84
Precision	0.98	0.98	0.99	0.89	0.97	0.96	0.87
Recall	0.89	0.85	0.94	0.89	0.92	0.93	0.81
Total	121 (110)	67 (63)	92 (88)	52 (54)	105 (101)	112 (110)	31 (30)
% Dead	0	73	0	77	1	0	52
Height	13.43	21.51	11.90	27.10	20.66	23.91	19.92
% Gap	56	64	52	55	65	68	89
Background	1	1	1, 4	1, 4	1	1	1, 2, 4
	2022						
F1-Score	0.94	0.81	0.81	0.75	0.00	0.96	0.90
Precision	0.96	0.75	0.86	0.77	0.00	0.98	0.81
Recall	0.91	0.88	0.78	0.74	0.00	0.94	1.00
Total	113 (107)	17 (20)	76 (69)	27 (26)	0 (11)	104 (100)	22 (27)
% Dead	0	35	93	19	0	99	5
Height	16.34	6.57	12.36	5.78	0.00	23.81	7.23
% Gap	66	94	62	93	100	66	94
Background	1	2, 3	1, 3	2, 4	3	1	2, 3, 4

(0.91 F1-Score, 0.80 AP), and lastly 2022 (0.88 F1-Score, 0.81 AP). The trend is mirrored in the overall Precision and Recall values, with Precision consistency slightly higher (0.88–0.96) than Recall (0.88–0.90) across all years. Looking at individual tree crown classes, the model performed slightly better at detecting alive trees compared to dead trees based on F1-Score and AP. However, in 2016, the F1-Score values were identical for both classes, and the AP was even higher for dead trees. The model exhibited a trend of higher Precision than Recall for alive tree crowns, whereas the opposite was true for dead tree crowns. Fig. 7 depicts the relationship between IoU and F1-Score. The curves for all three years demonstrate a similar trend: a relatively constant F1-Score up to an IoU of 0.7, followed by a steeper decline until reaching an F1-Score of 0 at an IoU of 0.95. The most stable performance was observed in 2016, followed by 2009. In 2022, the F1-Score dropped more significantly even at an IoU value of 0.6. Additionally, in 2009 and 2016, the accuracy for dead tree crowns declined more rapidly compared to live trees. Interestingly, in 2022, all curves exhibited a similar trend.

Table 6 presents the accuracy metrics and forest parameters for each validation plot. The details of these plots are visualized in Fig. A.11. Forest parameters show substantial changes between years due to forest development. Except for plot 5 in 2022, all plots achieved high accuracy with F1-Scores exceeding 0.75. Some interesting relationships emerge between forest parameters and validation metrics. Plots with high stand density, which translates to shaded backgrounds in the imagery, yielded the best results (Plots 1, 3, 5, and 6 in Table 6 for 2009 and 2016). These plots often exhibited a slight underestimation of tree crowns, indicated by a lower Recall than Precision. This phenomenon is evident in plots like 5 (2009), 3 (2016), and 1 (2022). Conversely, plots with a low number of trees, a high proportion of gaps, short tree heights, and uneven backgrounds led to lower accuracy. This resulted in more frequent overestimation, reflected in a higher Recall than Precision. Examples include plots 4 (2016), 2 (2022), and 7 (2022). Interestingly, the proportion of dead trees did not appear to affect the accuracy metrics.

4.2. Forest changes

Fig. 8 reveals considerably smaller changes in tree cover between 2009 (a) and 2016 (b) compared to the period between 2016 (b) and 2022 (c). In 2009 (a), there were barely any areas with dead trees. However, by 2016 (b), several smaller patches of dead trees emerged, particularly in the northwest region (Fig. 8b). This is reflected in the numerical data (Fig. 8d): the total number of trees between 2009 and 2016 remained relatively stable, increasing slightly from 749,618 to 755,340 (+0.76%). However, the number of alive trees decreased by 2.97%, while the number of dead trees increased by 215.01%. Comparing the 2016 (b) and 2022 (c) maps in Fig. 8, it is evident that large areas of trees have died or fallen. Fig. 8d confirms this observation. The total number of trees declined from 755,340 to 409,982 (−45.72%). The number of dead trees rose sharply (+268.39%), and the number of live trees dropped substantially (−63.48%). Overall, from 2009 to 2022, the total number of trees decreased by 45.31% (from 749,618 to 409,982). The number of alive trees declined even more (64.57%, from 736,786 to 261,072), while the number of dead trees increased by a substantial 1060.46% (from 12,832 to 148,910).

The maps in Fig. 9 of 2009 (a) and 2016 (c) showing a similar height structure: Areas with low height in the west and east centers of the area, as well as in the south. These structures were similar in both 2009 and 2016, but the 2016 map reveals more gaps in the forest. The histogram for alive trees in 2009 (b) showed two local maxima, one at about 25m and one at about 10m tree height, while the number dead trees was barely noticeable. In the histogram for alive trees in 2016 (d), the double local maximum was only slightly visible, as the larger maximum remained the same, while the smaller maximum increased. The curve of

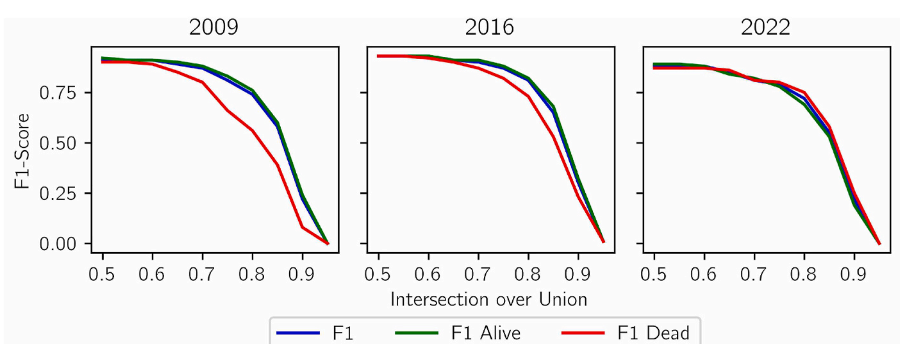

Fig. 7. The Relationship between intersection over union (IoU) and F1-Score of alive and dead tree crowns, as well as for total classification, for the years 2009, 2016 and 2022.

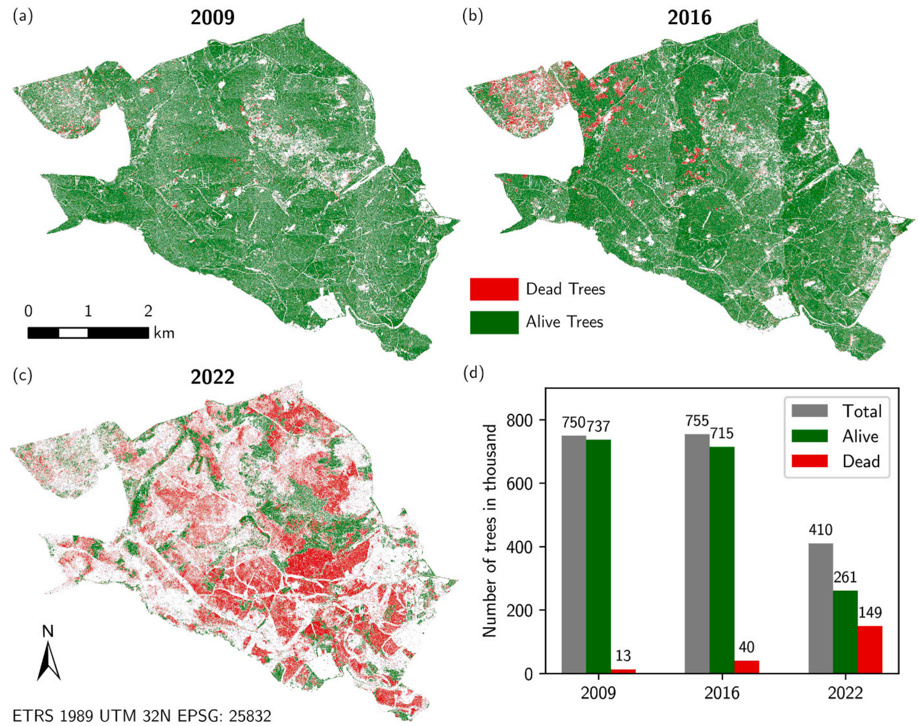

Fig. 8. Map of alive and dead trees for the years 2009 (a), 2016 (b) and 2022 (c). Histogram (d) shows the total number of detected alive and dead trees for the years 2009, 2016 and 2022.

dead trees was more evident here. Comparing the 2022 (e) to 2016 (c) map, low tree heights were found in the major part instead of the predominantly high tree heights. Areas without tree height were observed, particularly at the edges of the study area. When comparing histograms of 2016 (d) and 2022 (f), it is interesting to note that the structure of these double maximum values is also present here. The upper maximum value of the alive trees histograms in 2009 (b) and 2016 (d) could be found as the maximum in the dead trees histogram of 2022 (f) and the lower maximum value was visible in the alive trees. Additionally, there was a spike in the dead trees at very low tree heights and a spur in the alive trees at higher tree heights. Striking in the Figs. 8 and 9 are the strip effects in 2009 (a) in the horizontal and 2016 (c) in the vertical direction (for more details: 5.1).

5. Discussion

5.1. Tree detection and delineation performance

The accuracy assessment yields good performance of the Mask R–CNN with a F1-Score > 0.88 and an AP > 0.8. Furthermore, the Mask R–CNN was applied to images from three flight campaigns, each with different acquisition dates, cameras, post-processing, and tilting effects. The stable and high accuracy scores underline the transferability and reliability of this method. The analysis of performance at different IoU values in Fig. 7 showed that the model achieved a decent detection quality. Alive tree crowns were slightly better detected than dead tree crowns (Figs. 5 and 7). Reasons for the lower accuracy for dead trees might be the challenging separation between bare ground and dead trees, their less frequent occurrence in 2009 and 2016, and lower number of training samples. Table 5 and Fig. 7 also demonstrate that the classification in 2016 is more accurate than in 2009 and 2022, which can be attributed to a higher number of training samples from 2016. The accuracy metrics in 2022 indicate worse results than in 2009, although more training data was available in 2022. This is probably due to the more inhomogeneous forest structure with a higher number of dead trees in 2022. When considering Precision and Recall values, it can be concluded that there was an underestimation in the number of alive tree crowns and an overestimation of dead tree crowns. The underestimation of alive tree crowns is probably due to a lack of generalizability of the model and thus an insufficient number of training data. Comparable studies revealed that this is probably a widespread phenomenon (Beloiu et al., 2023; Chadwick et al., 2020; Natesan et al., 2020). For dead tree crowns, this is due to a higher number of false positives. The model was not able to rely on the CHM for dead trees as they were occasionally undetected in the stereomatching procedure.

A direct comparison to other studies is challenging, for example due to different input imagery, reference data, and environmental factors, such as the complexity of the forest environment (Zhao et al., 2023a; Zhang et al., 2022). Chadwick et al. (2020) demonstrates the detection of regenerating conifers in a single class in Canada using Mask R–CNN, achieving an F1-Score of 0.91 with the pretrained COCO network. Another study conducted in subtropical China detected and classified five broadleaf and three conifer tree species, achieving an F1-Score of 0.90–0.92 for conifers by using a very large training dataset with 52,737 manually delineated tree crowns (Zhang et al., 2022). Both studies demonstrate very similar accuracies for alive tree crowns (0.90–0.92) compared to those achieved with this method (0.89–0.93). Chiang et al. (2020) classified dead tree crowns in a single class surrounded by forest using Mask R–CNN, achieving a slightly lower AP of 0.6 than with this methodology (0.7–0.9), highlighting the difficulty in classifying dead tree crowns.

Although most of these studies differ slightly in spatial resolution, pretrained networks, number of training samples and detected classes, the presented results are in accordance with the results of other studies in terms of the accuracy.

The analysis of individual validation plots shows that a uniformly dense stand density and shadows as backgrounds, led to the best results. In contrast, inhomogeneous plots with small trees, lower stand density and forest gaps gave poorer results. A review paper by Zhao et al. (2023a) supports these findings: a heterogeneous background led to a more complex classification task, which required more training data. In some cases, bare ground was confused with dead trees, probably due to

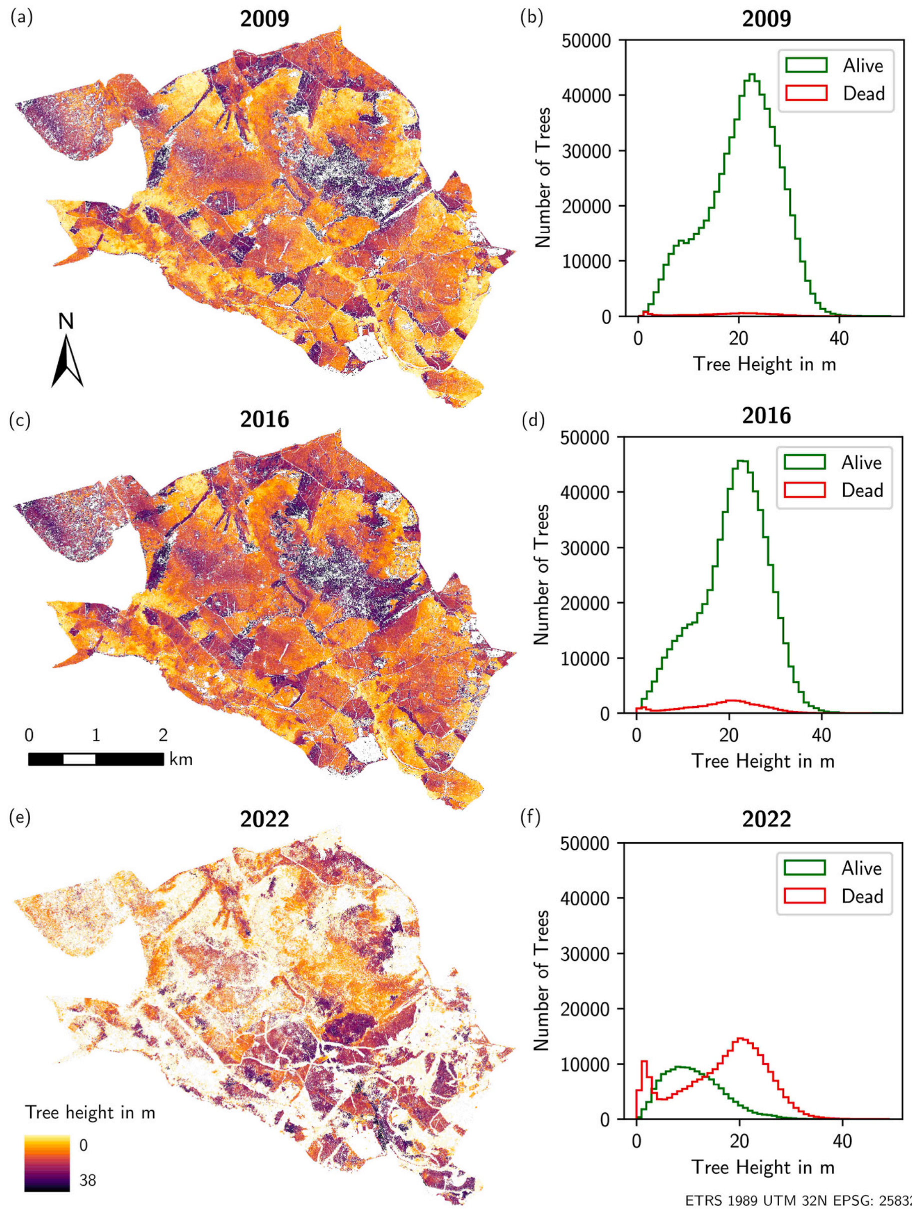

Fig. 9. Map of tree height for the years 2009 (a) 2016 (c) and 2022 (e). Histograms of the height for alive and dead trees for the respective years 2009 (b), 2016 (d) and 2022 (f).

their similar spectral composition.

The interpretation of the results shows some limitations of the proposed methodology: a strip pattern is visible in Figs. 8 and 9 in the years 2009 and 2016 and in detail in the Fig. B.12, which is due to the digital orthomosaic creation procedure and a lower long image overlap. This results in changing tilting effects and lighting, causing the detection to differ between the two sites. This strip pattern does not appear in 2022, which is due to a more sophisticated derivation of the orthophotos. True Orthophotos should be used for future analyses to avoid this effect. The photogrammetric derivation of CHM was already validated by Chadwick et al. (2020); Hao et al. (2021); Kirchhöfer et al. (2020a) and showed good internal height accuracies (<0.24m). However, missing height values for dead trees caused a spike at very low heights in the histograms of dead trees within Fig. 9. This is only slightly visible in 2009 and 2016 due to the low number of dead trees but is more pronounced in 2022. The training and validation data used here were produced solely on the basis of orthophotos, which in some cases makes it difficult to distinguish the crowns from one another. In addition, the data acquisition was only carried out by a single person, which can lead to a certain influence on the results despite the strictest diligence.

5.2. Forest changes

Considering the Figs. 8 and 9, a pattern can be identified. There were minor changes between 2009 and 2016, but from 2016 to 2022, major changes occurred. The small increase in alive trees from 2009 to 2016 could be attributed to a higher detection accuracy in 2016. From 2016 to 2022 a severe forest dieback was detected, with a loss of 63.48% of alive tree crowns and a simultaneous gain of 268.39% of dead tree crowns. The results show that the old and tall spruce stands were particularly affected by the forest dieback. This observation was also confirmed by the Harz National Park and the town of Osterrode (Harz National Park, 2022; Buff, 2021).

The forest loss can mainly be attributed to an outbreak of bark beetle infestation, which was particularly severe in the years 2018–2020 (Harz National Park, 2020b; Rohde et al., 2021). Such insect infestations have become more frequent in recent years due to climate change (Diez et al., 2021). In the Harz Mountains, three factors facilitated the spread of bark beetles and thus contributed to the severity of its destruction. The mountain range was forested with about 80% spruce, which provided a rich wood supply and enabled easy spreading (Schmidt et al., 2022). Additionally, there was a pronounced drought period in these years (Deutscher Wetterdienst, 2023a,b), which weakened the of trees' ability to resist the infestation (Rohde et al., 2021). This was exacerbated by the fact that the National Park only used mechanical insect control on 40% of its area in 2016, as it is restricted by strict nature conservation laws (Harz National Park, 2020b). The bark beetle was able to spread over a wide area and appeared in high quantities. To protect surrounding forest owners from the bark beetle swarms, a 500m wide protective strip was cleared along the edges of the national park (Harz National Park, 2020a). Moreover, additional areas were cleared of dead trees due to visitor protection or wildfire prevention as evident in Figs. 8 and 9 (Harz National Park, 2022).

6. Conclusion

This study evaluates the effectiveness of Mask R–CNN for individual tree detection and crown delineation in monitoring a forest dieback in the Harz Mountains. Therefore, a Mask R–CNN was used to delineate and classify trees as dead or alive, using aerial imagery and a canopy height model. The classified tree crowns were then used to analyze forest changes from 2009 to 2022, considering number, spatial distribution, and height.

The detailed accuracy assessment underlines the general good performance of Mask R–CNN. It effectively delineates individual tree crowns, and classifies them as dead or alive, even under varying conditions. This includes using aerial images with differing cameras, dates, post-processing and tilting effects. While the results indicate a slight underestimation of the total tree count, with a tendency to underestimate live trees and overestimate dead trees, accuracies remained stable throughout the study period. Between 2009 and 2016, no meaningful forest change was observed. However, substantial changes were identified between 2016 and 2022. Overall, a severe forest dieback was detected, with a total loss of 64.57% of living trees. Notably, tall trees were disproportionately affected.

This study demonstrates the potential of ITDCD using Mask R–CNN on aerial imagery as a valuable tool for forest dieback monitoring. Future research could focus on incorporating True Orthophotos and very high-resolution satellite imagery to establish more consistent and frequent monitoring.

The integration of these results could lay the groundwork for automated forest monitoring systems. Such systems could provide real-time or near-real-time updates on forest inventory and health, facilitating timely intervention and management strategies.

CRediT authorship contribution statement

Moritz Lucas: Writing – review & editing, Writing – original draft, Visualization, Validation, Methodology, Investigation, Formal analysis, Data curation, Conceptualization. **Maren Pukrop:** Writing – review & editing, Writing – original draft, Supervision, Methodology, Conceptualization. **Philip Beckschäfer:** Writing – review & editing, Supervision, Software, Resources, Conceptualization. **Björn Waske:** Writing – review & editing, Writing – original draft, Supervision, Methodology, Conceptualization.

Acknowledgments

The authors would like to express their gratitude to the Harz National Park and the Northwest German Forest Research Institute for providing the data. We would especially be grateful to Ute Springemann for her valuable guidance regarding the local environment and flora in the Harz National Park.

Appendix A. Training- and Validationplot Details

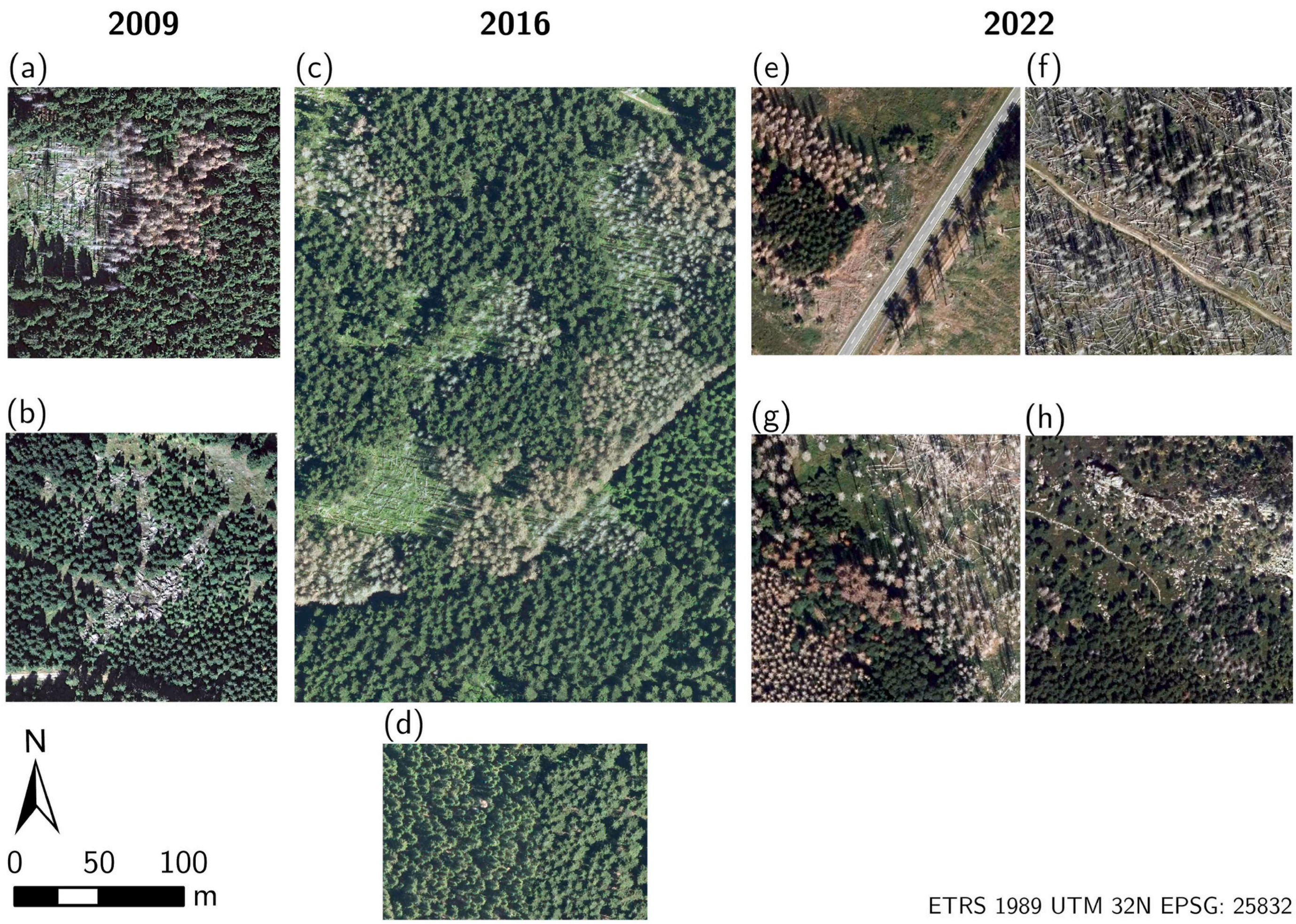

Fig. A.10. Details of the training plots used in each year, along with the corresponding aerial imagery as an RGB composite. The location of these polygons can be seen in Fig. 3.

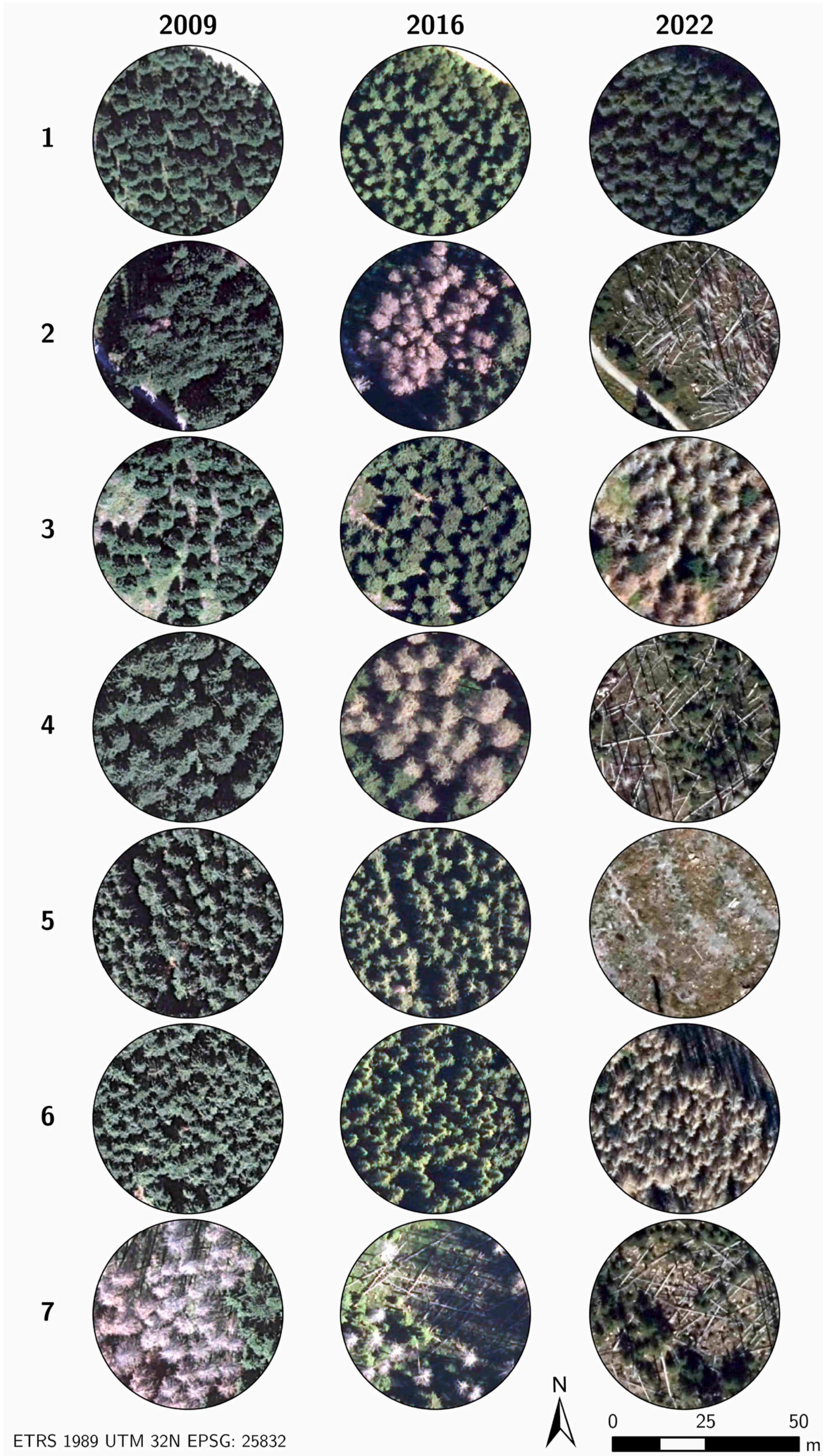

Fig. A.11. Details of the validation plots used in each year with the corresponding aerial imagery as an RGB composite. The location can be seen in Fig. 3.

Appendix B. Strip Pattern Detail

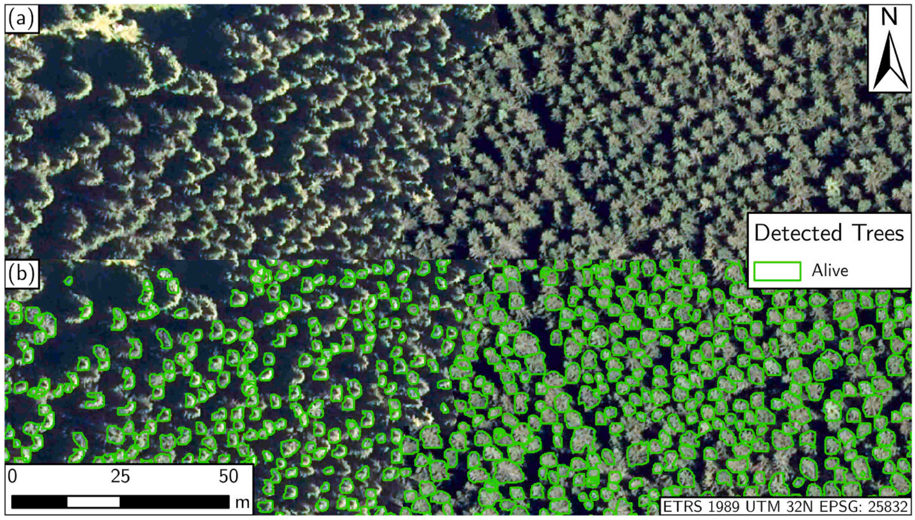

Fig. B.12. Details of the strip pattern in 2016 (a) with aerial imagery and (b) with added detected trees.

References

Bagheri, N., Kafashan, J., 2023. Uav-based remote sensing in orcha-forest environment; diversity of research, used platforms and sensors. Remote Sens. Appl.: Society and Environment 32, 101068. https://doi.org/10.1016/j.rsase.2023.101068.

Beloiu, M., Heinzmann, L., Rehush, N., Gessler, A., Griess, V.C., 2023. Individual tree-crown detection and species identification in heterogeneous forests using aerial rgb imagery and deep learning. Rem. Sens. 15 https://doi.org/10.3390/rs15051463.

Braga, J.R.G., Peripato, V., Dalagnol, R., Ferreira, M.P., Tarabalka, Y.O.C., Aragão, L.E., de Campos Velho, H.F., Shiguemori, E.H., Wagner, F.H., 2020. Tree crown delineation algorithm based on a convolutional neural network. Rem. Sens. 12 https://doi.org/10.3390/rs12081288.

Buff, R., 2021. Städtischer Waldbesitz seit 500 Jahren: Auswirkungen der Klimaveränderungen für die Stadt Osterode am Harz und ihren Wald. Stadtforschung und Statistik. Zeitschrift des Verbandes Deutscher Städtestatistiker 34, 2–7.

Chadwick, A.J., Goodbody, T.R.H., Coops, N.C., Hervieux, A., Bater, C.W., Martens, L.A., White, B., Röeser, D., 2020. Automatic delineation and height measurement of regenerating conifer crowns under leaf-off conditions using uav imagery. Rem. Sens. 12 https://doi.org/10.3390/rs12244104.

Chiang, C.Y., Barnes, C., Angelov, P., Jiang, R., 2020. Deep learning-based automated forest health diagnosis from aerial images. IEEE Access 8, 144064–144076. https://doi.org/10.1109/ACCESS.2020.3012417.

Dersch, S., Schöttl, A., Krzystek, P., Heurich, M., 2023. Towards complete tree crown delineation by instance segmentation with mask r–cnn and detr using uav-based multispectral imagery and lidar data. ISPRS Open J. Photogramm. Rem. Sens. 8, 100037 https://doi.org/10.1016/j.ophoto.2023.100037.

Deutscher Wetterdienst, 2023a. Annual Average of Station Measurements of Air Temperature at a Height of 2 M in Celsius for germany. https://cdc.dwd.de/portal/202209231028/mapview. (Accessed 27 November 2023).

Deutscher Wetterdienst, 2023b. Annual Sum of Station Measurements of Precipitation in Mm for germany. https://cdc.dwd.de/portal/202209231028/mapview. (Accessed 27 November 2023).

Diez, Y., Kentsch, S., Fukuda, M., Caceres, M.L.L., Moritake, K., Cabezas, M., 2021. Deep learning in forestry using uav-acquired rgb data: a practical review. Rem. Sens. 13 https://doi.org/10.3390/rs13142837.

Gibril, M.B.A., Shafri, H.Z.M., Shanableh, A., Al-Ruzouq, R., Wayayok, A., bin Hashim, S. J., Sachit, M.S., 2022. Deep convolutional neural networks and swin transformer-based frameworks for individual date palm tree detection and mapping from large-scale uav images. Geocarto Int. 37, 18569–18599. https://doi.org/10.1080/10106049.2022.2142966.

Hao, Z., Lin, L., Post, C.J., Mikhailova, E.A., Li, M., Chen, Y., Yu, K., Liu, J., 2021. Automated tree-crown and height detection in a young forest plantation using mask region-based convolutional neural network (mask r-cnn). ISPRS J. Photogrammetry Remote Sens. 178, 112–123. https://doi.org/10.1016/j.isprsjprs.2021.06.003.

Hao, Z., Post, C.J., Mikhailova, E.A., Lin, L., Liu, J., Yu, K., 2022. How does sample labeling and distribution affect the accuracy and efficiency of a deep learning model for individual tree-crown detection and delineation. Rem. Sens. 14 https://doi.org/10.3390/rs14071561.

Harz National Park, 2020a. Borkenkäferbekämpfung an der Nationalparkgrenze intensiviert. https://www.nationalpark-harz.de/de/aktuelles/2020/2020_06_12_Borkenkaefersicherung/. (Accessed 6 June 2024).

Harz National Park, 2020b. Waldentwicklung im Nationalpark Harz. https://www.nationalpark-harz.de/de/downloads/Waldentwicklung-im-Nationalpark-Harz?download=barrierearm. (Accessed 6 June 2024).

Harz National Park, 2022. Tätigkeitsbericht 2021. https://s.gwdg.de/0mlA9D. (Accessed 6 June 2024).

Harz National Park, 2023a. Tätigkeitsbericht 2022. https://s.gwdg.de/d6O0RT. (Accessed 6 June 2024).

Harz National Park, 2023b. Wir über uns. https://www.nationalpark-harz.de/de/der-nationalpark-harz/wir-ueber-uns/. (Accessed 6 June 2024).

He, K., Gkioxari, G., Dollár, P., Girshick, R., 2020. Mask r-cnn. IEEE Trans. Pattern Anal. Mach. Intell. 42, 386–397. https://doi.org/10.1109/TPAMI.2018.2844175.

Holzwarth, S., Thonfeld, F., Abdullahi, S., Asam, S., Da Ponte Canova, E., Gessner, U., Huth, J., Kraus, T., Leutner, B., Kuenzer, C., 2020. Earth observation based monitoring of forests in Germany: a review. Rem. Sens. 12 https://doi.org/10.3390/rs12213570.

Holzwarth, S., Thonfeld, F., Kacic, P., Abdullahi, S., Asam, S., Coleman, K., Eisfelder, C., Gessner, U., Huth, J., Kraus, T., Shatto, C., Wessel, B., Kuenzer, C., 2023. Earth-observation-based monitoring of forests in Germany - recent progress and research frontiers: a review. Rem. Sens. 15 https://doi.org/10.3390/rs15174234.

Jaskierniak, D., Lucieer, A., Kuczera, G., Turner, D., Lane, P., Benyon, R., Haydon, S., 2021. Individual tree detection and crown delineation from unmanned aircraft system (uas) lidar in structurally complex mixed species eucalypt forests. ISPRS J. Photogrammetry Remote Sens. 171, 171–187. https://doi.org/10.1016/j.isprsjprs.2020.10.016.

Ke, Y., Quackenbush, L.J., 2011. A review of methods for automatic individual tree-crown detection and delineation from passive remote sensing. Int. J. Rem. Sens. 32, 4725–4747. https://doi.org/10.1080/01431161.2010.494184.

Kirchhöfer, M., Beckschäfer, P., Adler, P., Ackermann, J., 2020a. Ableitung von Oberflächenmodellen aus Luftbildern – das Verfahren des F^3 Projektes. https://www.waldwissen.net/de/technik-und-planung/waldinventur/ableitung-von-oberflaechenmodellen-aus-luftbildern#c105648. (Accessed 6 June 2024).

Kirchhöfer, M., Beckschäfer, P., Adler, P., Ackermann, J., 2020b. Walddaten für eine moderne, nachhaltige Forstwirtschaft. https://www.waldwissen.net/de/technik-und-planung/waldinventur/f3-fernerkundungsbasierte-walddaten. (Accessed 6 June 2024).

Kison, H.U., Ciongwa, P., Czichowski, H.J., Hammelsbeck, U., Herdam, H., Illig, W., Karste, G., Sprick, P., Thiel, H., Wegener, U., 2020. Flora des Nationalparks Harz. Schriftenreihe aus dem Nationalpark Harz 554–570.

Knapp, H., Robin, V., Kirleis, W., Nelle, O., 2013. Woodland history in the upper harz mountains revealed by kiln site, soil sediment and peat charcoal analyses. Quat. Int. 289, 88–100. https://doi.org/10.1016/j.quaint.2012.03.040.

Lassalle, G., Ferreira, M.P., La Rosa, L.E.C., de Souza Filho, C.R., 2022. Deep learning-based individual tree crown delineation in mangrove forests using very-high-resolution satellite imagery. ISPRS J. Photogrammetry Remote Sens. 189, 220–235. https://doi.org/10.1016/j.isprsjprs.2022.05.002.

Li, K., Wan, G., Cheng, G., Meng, L., Han, J., 2020. Object detection in optical remote sensing images: a survey and a new benchmark. ISPRS J. Photogrammetry Remote Sens. 159, 296–307. https://doi.org/10.1016/j.isprsjprs.2019.11.023.

Li, Y., Chai, G., Wang, Y., Lei, L., Zhang, X., 2022. Ace r-cnn: an attention complementary and edge detection-based instance segmentation algorithm for individual tree species identification using uav rgb images and lidar data. Rem. Sens. 14 https://doi.org/10.3390/rs14133035.

Lucena, F., Breunig, F.M., Kux, H., 2022. The combined use of uav-based rgb and dem images for the detection and delineation of orange tree crowns with mask r-cnn: an approach of labeling and unified framework. Future Internet 14. https://doi.org/10.3390/fi14100275.

Maxwell, A.E., Warner, T.A., Guillén, L.A., 2021. Accuracy assessment in convolutional neural network-based deep learning remote sensing studies—part 1: literature review. Rem. Sens. 13 https://doi.org/10.3390/rs13132450.

Mielczarek, D., Sikorski, P., Archicinski, P., Ciezkowski, W., Zaniewska, E., Chormański, J., 2023. The use of an airborne laser scanner for rapid identification of invasive tree species acer negundo in riparian forests. Rem. Sens. 15 https://doi.org/10.3390/rs15010212.

Minařík, R., Langhammer, J., Lendzioch, T., 2020. Automatic tree crown extraction from uas multispectral imagery for the detection of bark beetle disturbance in mixed forests. Rem. Sens. 12 https://doi.org/10.3390/rs12244081.

Mohan, M., Silva, C.A., Klauberg, C., Jat, P., Catts, G., Cardil, A., Hudak, A.T., Dia, M., 2017. Individual tree detection from unmanned aerial vehicle (uav) derived canopy height model in an open canopy mixed conifer forest. Forests 8. https://doi.org/10.3390/f8090340.

Natesan, S., Armenakis, C., Vepakomma, U., 2020. Individual tree species identification using dense convolutional network (densenet) on multitemporal rgb images from uav. J. Unmanned Veh. Syst. 8, 310–333. https://doi.org/10.1139/juvs-2020-0014.

Nduji, N.N., Tolpekin, V.A., Stein, A., 2023. An object-based image analysis approach for comparing tree detection from satellite imagery at different scales; a case study in sukumba Mali. Remote Sens. Appl.: Society and Environment 30, 100960. https://doi.org/10.1016/j.rsase.2023.100960.

Nguyen, H.T., Lopez Caceres, M.L., Moritake, K., Kentsch, S., Shu, H., Diez, Y., 2021. Individual sick fir tree (abies mariesii) identification in insect infested forests by means of uav images and deep learning. Rem. Sens. 13 https://doi.org/10.3390/rs13020260.

Padilla, R., Netto, S.L., da Silva, E.A.B., 2020. A survey on performance metrics for object-detection algorithms. In: 2020 International Conference on Systems, Signals and Image Processing (IWSSIP), pp. 237–242. https://doi.org/10.1109/IWSSIP48289.2020.9145130.

Ren, S., He, K., Girshick, R., Sun, J., 2017. Faster r-cnn: towards real-time object detection with region proposal networks. IEEE Trans. Pattern Anal. Mach. Intell. 39, 1137–1149. https://doi.org/10.1109/TPAMI.2016.2577031.

Rohde, M., Langer, G., Hurling, R., Plašil, P., 2021. Waldschutzsituation 2020 in nordwestdeutschland. AFZ-Wald 76, 42–46.

Safonova, A., Guirado, E., Maglinets, Y., Alcaraz-Segura, D., Tabik, S., 2021. Olive tree biovolume from uav multi-resolution image segmentation with mask r-cnn. Sensors 21. https://doi.org/10.3390/s21051617.

Safonova, A., Tabik, S., Alcaraz-Segura, D., Rubtsov, A., Maglinets, Y., Herrera, F., 2019. Detection of fir trees (abies sibirica) damaged by the bark beetle in unmanned aerial vehicle images with deep learning. Rem. Sens. 11 https://doi.org/10.3390/rs11060643.

Sandric, I., Irimia, R., Petropoulos, G.P., Anand, A., Srivastava, P.K., Pleșoianu, A., Faraslis, I., Stateras, D., Kalivas, D., 2022. Tree's detection & health's assessment from ultra-high resolution uav imagery and deep learning. Geocarto Int. 37, 10459–10479. https://doi.org/10.1080/10106049.2022.2036824.

Schiefer, F., Kattenborn, T., Frick, A., Frey, J., Schall, P., Koch, B., Schmidtlein, S., 2020. Mapping forest tree species in high resolution uav-based rgb-imagery by means of convolutional neural networks. ISPRS J. Photogrammetry Remote Sens. 170, 205–215. https://doi.org/10.1016/j.isprsjprs.2020.10.015.

Schmidt, M., Lorenz, K., Mölder, A., 2022. Die Wälder des Harzes. Ornithol. Jber. Mus. Heineanum 36, 3–12.

Smith, L.N., 2017. Cyclical learning rates for training neural networks. In: 2017 IEEE Winter Conference on Applications of Computer Vision (WACV), pp. 464–472doi. https://doi.org/10.1109/WACV.2017.58.

Sun, Y., Li, Z., He, H., Guo, L., Zhang, X., Xin, Q., 2022. Counting trees in a subtropical mega city using the instance segmentation method. Int. J. Appl. Earth Obs. Geoinf. 106, 102662 https://doi.org/10.1016/j.jag.2021.102662.

Sun, Z., Wang, Y.f., Ding, Z.d., Liang, R.t., Xie, Y.h., Li, R., Li, H.w., Pan, L., Sun, Y.j., 2023. Individual tree segmentation and biomass estimation based on uav digital aerial photograph. J. Mt. Sci. 20, 724–737. https://doi.org/10.1007/s11629-022-7563-7.

Thonfeld, F., Gessner, U., Holzwarth, S., Kriese, J., da Ponte, E., Huth, J., Kuenzer, C., 2022. A first assessment of canopy cover loss in germanys forests after the 2018-2020 drought years. Rem. Sens. 14 https://doi.org/10.3390/rs14030562.

Trimble, 2019. Match-3dx, Match-T Dsm Manual for Version 9.2 and Higher.

Wagner, F.H., Ferreira, M.P., Sanchez, A., Hirye, M.C., Zortea, M., Gloor, E., Phillips, O. L., de Souza Filho, C.R., Shimabukuro, Y.E., Aragão, L.E., 2018. Individual tree crown delineation in a highly diverse tropical forest using very high resolution satellite images. sI: Latin America Issue ISPRS J. Photogrammetry Remote Sens. 145, 362–377. https://doi.org/10.1016/j.isprsjprs.2018.09.013.

Wu, G., Li, Y., 2021. Non-maximum suppression for object detection based on the chaotic whale optimization algorithm. J. Vis. Commun. Image Represent. 74, 102985 https://doi.org/10.1016/j.jvcir.2020.102985.

Yang, M., Mou, Y., Liu, S., Meng, Y., Liu, Z., Li, P., Xiang, W., Zhou, X., Peng, C., 2022. Detecting and mapping tree crowns based on convolutional neural network and google earth images. Int. J. Appl. Earth Obs. Geoinf. 108, 102764 https://doi.org/10.1016/j.jag.2022.102764.

Yu, K., Hao, Z., Post, C.J., Mikhailova, E.A., Lin, L., Zhao, G., Tian, S., Liu, J., 2022. Comparison of classical methods and mask r-cnn for automatic tree detection and mapping using uav imagery. Rem. Sens. 14 https://doi.org/10.3390/rs14020295.

Zhang, C., Zhou, J., Wang, H., Tan, T., Cui, M., Huang, Z., Wang, P., Zhang, L., 2022. Multi-species individual tree segmentation and identification based on improved mask r-cnn and uav imagery in mixed forests. Rem. Sens. 14 https://doi.org/10.3390/rs14040874.

Zhao, H., Morgenroth, J., Pearse, G., Schindler, J., 2023a. A systematic review of individual tree crown detection and delineation with convolutional neural networks (cnn). Curr. Forest. Rep. 9, 149–170. https://doi.org/10.1007/s40725-023-00184-3.

Zhao, H., Morgenroth, J., Pearse, G., Schindler, J., 2023b. A systematic review of individual tree crown detection and delineation with convolutional neural networks (cnn). Curr. Forest. Rep. 9, 149–170. https://doi.org/10.1007/s40725-023-00184-3.

Zhen, Z., Quackenbush, L.J., Zhang, L., 2016. Trends in automatic individual tree crown detection and delineation—evolution of lidar data. Rem. Sens. 8 https://doi.org/10.3390/rs8040333.